ELSEVIER

Applied Surface Science 108 (1997) 257–262

applied surface science

Bistabilities in pyrolytic laser-CVD of silicon and carbon

P.B. Kargl, N. Arnold *, D. Bäuerle

Angewandte Physik, Johannes-Kepler-Universität Linz, A-4040 Linz, Austria

Received 6 May 1996; accepted 30 July 1996

Abstract

In pyrolytic laser-CVD of silicon and carbon, bistable growth with a pronounced hysteresis was observed within certain regimes of scanning velocities and laser powers. In order to study the influence of changes in heat conductivities and activation energy, we have deposited onto different substrate materials silicon from SiH_4 and Si_2H_6 and carbon from CH_4, C_2H_2, and C_2H_4.

PACS: 42.60; 81.15; 82.00

1. Introduction

Laser direct writing is a single step technique for surface micropatterning [1]. Here, periodic structures and instabilities of different kinds have been observed for a large number of systems [2–13]. For most applications, structure formation is not desirable, since it limits the ultimate resolution achieved in the process. Recently, we have reported the first clear observation of bistable behavior during pyrolytic direct writing of Si lines deposited from silane by means of Ar^+-laser radiation [14]. Here, two regimes with different types of deposits have been observed: Uniform (continuous) lines and equidistant fibers. By changing either the scanning velocity or the laser power, an abrupt (Fig. 1a) or a smooth (Fig. 1b) transition between these regimes may occur. In the first case, the transition shows a hysteresis with increasing/decreasing laser power or scanning velocity. A theoretical model based on a one-dimensional approach for laser direct writing [15] was developed in order to explain the limits of continuous growth [16]. This model which takes into account the temperature gradient in z-direction (perpendicular to substrate) and the finite size of the laser focus, describes qualitatively the discontinuity in the deposition process. In order to further test the adequacy of this model, we have investigated the influences of the heat conductivities and the activation energy of the pyrolytic decomposition on the deposition process.

2. Experimental

The experimental setup for Si and C deposition was similar to that described in [17]. A CW Ar^+-laser operating at 514.5 nm was focused to a spot of $2w_0(1/e) = 5$ μm or $2w_0(1/e) = 3$ μm. As substrates we used platelets of glass, fused silica (a-

* Corresponding author.

0169-4332/97/$17.00 Copyright © 1997 Elsevier Science B.V. All rights reserved.
PII S0169-4332(96)00592-2

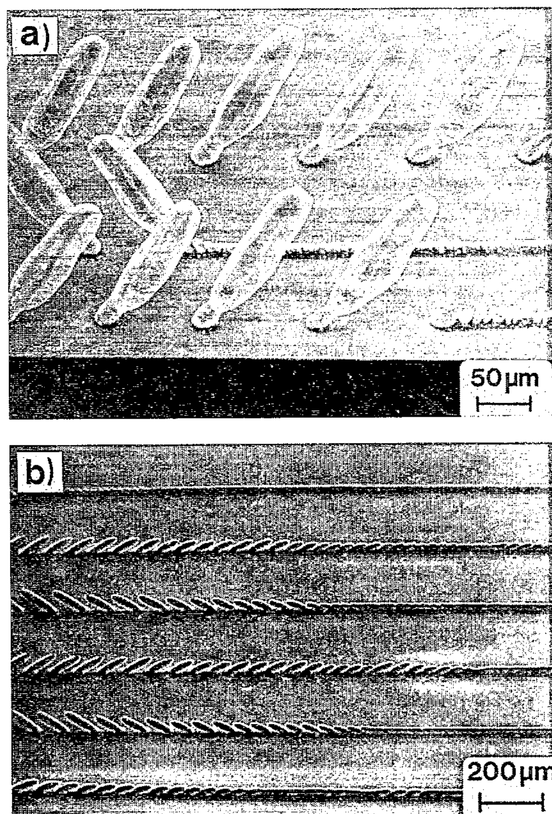

Fig. 1. (a) Scanning electron microscope (SEM) picture of silicon deposits fabricated by Ar^+-laser ($\lambda = 514.5$ nm, $2w_0 = 3$ μm) direct writing with increasing and decreasing scanning velocity. The picture was taken at an angle of 45°. The silane pressure was 500 mbar. For the lower and the upper trace the laser beam was scanned from left to right with a laser power of 136 mW and increasing velocity. For the trace in the middle, the beam was scanned from right to left with decreasing velocity. (b) Similar picture for C deposited from 1000 mbar C_2H_2 with $P = 150$ mW and $2w_0 = 3$ μm. The transition is almost smooth.

SiO_2), $SrTiO_3$, and (polished) ceramic ZrO_2 (YSZ). All of these substrates were covered with an about 100 nm thick layer of amorphous silicon (a-Si) which strongly absorbs the laser light and thereby permits well-defined initiation of the deposition process. For the observation of bistable behavior, the scanning velocity, v_s, was linearly increased or decreased. The precursors employed for deposition of Si were monosilane (SiH_4) and disilane (Si_2H_6), while C was deposited from ethyne (C_2H_2), ethene (C_2H_4), and methane (CH_4).

3. Results and discussion

Fig. 1a shows a scanning electron microscope (SEM) picture of a typical Si deposit. In the lower and upper part of the figure, v_s was continuously increased during scanning from left to right. In the middle, v_s was decreased during scanning from right to left. The laser power, P, and the gas pressure $p(SiH_4)$, were kept constant. The situation is similar if the laser power is increased or decreased during scanning with $v_s = \text{const.}$ [14].

In a v_s–P diagram one can separate two regions where only uniform lines or only fibers are obtained. Continuous deposition of lines is found only above a certain critical velocity $v_s^{cr} \approx W(T^{cr})$ where W denotes the growth rate which is given by the Arrhenius law $W = W_0 \exp(-\Delta E_A / k_B T)$. Within the one-dimensional model of laser direct writing [15,16], when the absorbed laser intensity is treated as a point source, the critical center temperature, T^{cr}, can be described by $T^{cr} \propto \Delta E_A / k_B \kappa^*$ [16]. Here, ΔE_A is the apparent activation energy and $\kappa^* = \kappa_D / \kappa_S$. κ_D and κ_S are the heat conductivities of the deposit and the substrate, respectively. Thus $v_s^{cr} \propto \exp(-\text{const.}\, \kappa_D / \kappa_S)$ and an increase in κ^* should shift the critical curve, which separates lines from fibers, to lower scanning velocities. More detailed calculations [16], which take into account the finite size of the laser spot, show that a decrease in ΔE_A has the same effect. The calculated shape of the critical curve is similar to that found in the experiments. The dependence of T^{cr} and v_s^{cr} on laser power is mainly due to the finite size of the laser spot. For high laser powers, when the width of the deposit is much larger than the laser spot, v_s^{cr} becomes almost independent of P.

To examine that, three types of experiments have been performed. First, κ^* was changed by varying the substrate material. Second, ΔE_A was changed by using as precursor disilane instead of silane. Third, deposition of C from different precursors has been investigated.

3.1. The influence of the substrate

Fig. 2 shows the critical curve for a-SiO_2 substrates covered with a-Si layers of various thicknesses, h_1. The silane pressure was 500 mbar. Each

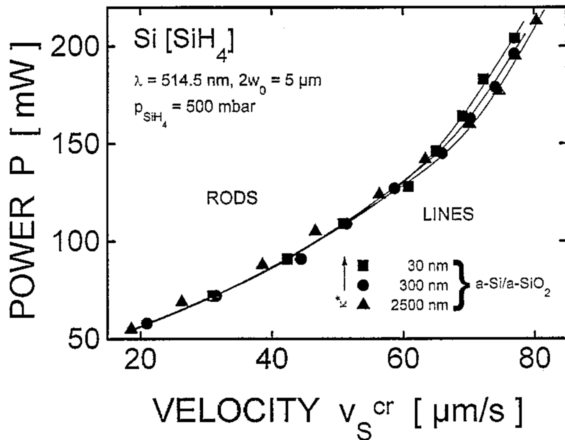

Fig. 2. Changes in the critical curve for SiH_4. Thicknesses of the a-Si layer on the a-SiO_2 substrate were varied.

point is an average of three values of v_s^{cr} obtained from double-scans with increasing and decreasing v_s at fixed laser power. The hysteresis effect is not shown in this figure, i.e., the median values of v_s^{cr} for ascending and descending scanning velocity were taken. The standard deviation for v_s^{cr} is about 2 μm/s. Because of the small influence of the a-Si layer on κ^*, the effect is small, but the trend agrees with the theoretical prediction that a decrease in κ^* increases T^{cr} and thereby v_s^{cr}.

Fig. 3 shows the results of similar experiments using different substrate materials. The corresponding heat conductivities are listed in Table 1. Above about 500°C the heat conductivity of ZrO_2 is lower than that of fused silica and the critical curve moves to the left. $SrTiO_3$ shows the same effect; thus, within the investigated temperature (power) interval, its heat conductivity should be below that of fused silica. The critical curve obtained in earlier experiments [14,16] using glass substrates covered with 120 nm a-Si exhibits a similar behavior.

Table 1
Heat conductivity κ for different materials and temperatures (from Ref. [18])

	κ (W m^{-1} K^{-1})			
	0°C	100°C	300°C	1000°C
a-SiO_2	1.35	1.42	1.70	3.3
c-Si	170	108	65	32 (700°C)
ZrO_2 ceramic		2.0	2.0	2.0
$SrTiO_3$	10.0			

3.2. The influence of the activation energy: silane and disilane

Fig. 4 shows critical curves for the deposition of Si from SiH_4 and Si_2H_6. In order to obtain similar deposition rates, we employed only 50 mbar of Si_2H_6. For an interpretation of these results, the kinetic constants ΔE_A and W_0 must be known. These parameters were determined from the Arrhenius plot in Fig. 5. Here, W was derived from the height of spots grown with different illumination

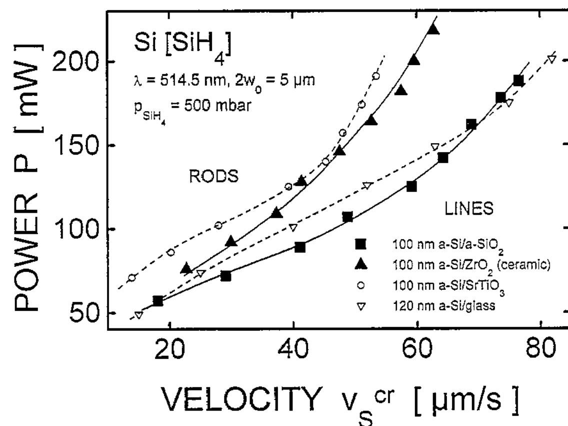

Fig. 3. Changes in the critical curve for SiH_4 for different substrates, all of them covered with a layer of about 100 nm a-Si.

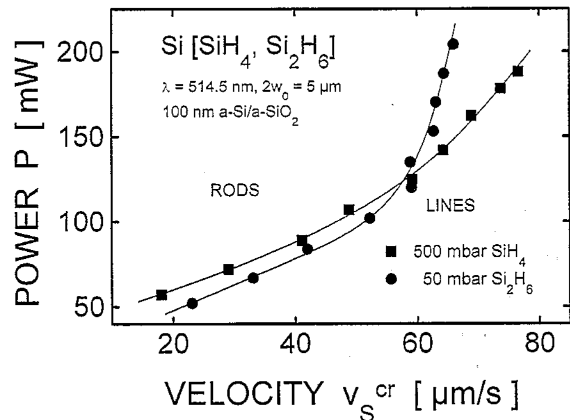

Fig. 4. Critical curves for Si deposited from SiH_4 and Si_2H_6.

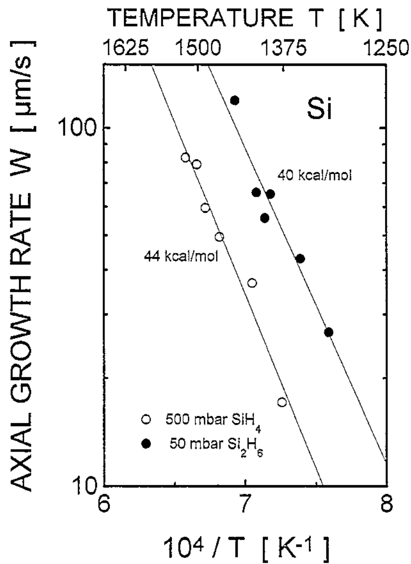

Fig. 5. Arrhenius plot for Si spots deposited from SiH_4, and Si_2H_6. The growth rate was determined experimentally. The temperatures were calculated. The full lines are least-squares fits to the data.

times. The temperature was calculated by using a fast algorithm for flat spots [19]. The height of spots which fitted our experimental data best, was approximated by $h(r) = h_0(1-(r/R)^3)$ with $h_0 < 2R$. The accuracy in the *linearized* temperature is quite satisfactory as long as $\kappa^* > 5$ [19]. The heat conductivity of Si depends strongly on temperature ($\kappa_{Si}(T) = k(T-T_k)^{-1}$, with $k = 2.99 \times 10^4$ W/m and $T_k = 99$ K). Thus, small errors in the linearized temperature, θ, which is calculated from the stationary heat conduction equation, can result in bigger errors in the temperature, $T \propto \exp\theta$. Least-squares fits to the data in Fig. 5 yield 44.3 ± 4 and 40.4 ± 5 kcal/mol for the apparent activation energies of silane and disilane, respectively. These values agree quite well with those found in the literature for SiH_4 (43.5 ± 1 kcal/mol [1]) and Si_2H_6 (42.75 ± 6.75 kcal/mol [20] and 38.0 kcal/mol [21]). The pre-exponential factors, W_0, for 500 mbar SiH_4 and 50 mbar Si_2H_6 are close to each other ($(2.0 \pm 0.5) \times 10^4$ cm/s and $(1.4 \pm 0.5) \times 10^4$ cm/s respectively, from Fig. 5).

At elevated powers, the critical curve for Si deposited from Si_2H_6 is shifted to the left with respect to that of SiH_4 (Fig. 4). The numerical calculations show, that this may be related to the slight difference in activation energies as mentioned in the beginning of this section. The details of the algorithm for the calculation of the critical curve in the v_s–P plane are given in [16]. They are based on the one-dimensional (in the direction of the deposited line) model for laser direct writing, which takes into account finite size of the laser spot and the temperature differences within the stripe in the direction perpendicular to the substrate. The decrease in v_s^{cr} (or *increase* in P^{cr} for fixed v_s) with decreasing activation energy may be illustrated by the following reasoning. Discontinuous deposition is observed at low v_s, which correspond to the small growth rates, i.e., to big ratios $\Delta E_A/k_B T$ [16]. If the activation energy ΔE_A decreases, as it is the case for the change from SiH_4 to Si_2H_6 as a precursor gas, this ratio decreases and the deposition becomes continuous. Therefore, the critical curve is shifted to a lower temperatures and scanning velocities. Note, that the deposition temperature *increases* with increasing v_s due to a decrease in the cross-section of the stripe, which is a good heat conductor [15,16].

The shift to the right observed for Si_2H_6 for low P may be due to the possible differences in the heat conductivities κ_D of the deposits from the two precursors in this region. As it follows from the numerical calculations [16] and is explained in the beginning of this section, a decrease in $\kappa^* = \kappa_D/\kappa_S$ shifts the critical curve to the right. For Si deposited from disilane higher H content (i.e., lower κ_D) is expected, because for equal v_s, which means *with equal growth rates*, the deposition from Si_2H_6 proceeds at *lower* temperatures (and thus significantly smaller hydrogen diffusion coefficients) due to the lower value of ΔE_A (see [22], and Fig. 5). While under equilibrium conditions practically no hydrogen is left in Si deposited above 500°C, the high cooling rates involved in laser CVD may result in hydrogen incorporation. The calculated deposition temperatures [19] are around 1400 K (see e.g., Fig. 5) and the heated zone in the deposited line is about 10 μm long. Thus, with $v_s \approx 10$ μm/s, the cooling time t is about 1 s. The diffusion coefficient of H in Si at these temperatures is $D \approx 10^{-8}$ cm^2/s [23]. Therefore, hydrogen can diffuse over a distance $(Dt)^{1/2} \approx 1$ μm which is *smaller* than the thickness of the deposit. This mechanism will lead to a different H

content for the deposition from silane and disilane only in the lower left corner of the Fig. 4, because for high P and v_s (high temperatures), D is big enough, and the hydrogen will completely evolve out of the deposit in both cases.

3.3. Carbon

Bistabilities have been observed also during direct writing of C lines from C_2H_2, C_2H_4, and CH_4. With C_2H_2, the transition from uniform lines to fibers is almost continuous with v_s and shows no hysteresis (Fig. 1b). This may be related to the fact that with the high critical velocity observed with C_2H_2 the fibers are strongly tilted. With C_2H_4 and CH_4, an abrupt transition from lines to fibers, which shows also a hysteresis, was observed. With both precursors the 'jump' is smaller than for Si. This can, in principle, again be related to the higher value of v_s^{cr}, and thereby the stronger tilt of fibers. Fig. 6 exhibits the critical curves for the different precursors.

In order to interpret these data we consider the activation energies, and the pre-exponential factors for the pressures employed: 43.5 kcal/mol, 0.1 cm/s for CH_4 ($T < 2800$ K); 47.3 kcal/mol, 3 cm/s for C_2H_2; and 58.3 kcal/mol, 140 cm/s for C_2H_4 [24]. A decrease in both ΔE_A and W_0 shifts the critical curve to lower velocities. Thus, with the assumption that the heat conductivities of the deposits are the same in all three cases, one expects $v_s^{cr}(CH_4) < v_s^{cr}(C_2H_2) < v_s^{cr}(C_2H_4)$. In the experiments, the last inequality is reversed, probably due to differences in the heat conductivities of C deposited from different precursors. The heat conductivity of pyrolytic carbon depends strongly on deposition temperature [25,23] and it is, like that of graphite, strongly anisotropic. Therefore, any quantitative considerations can hardly be performed.

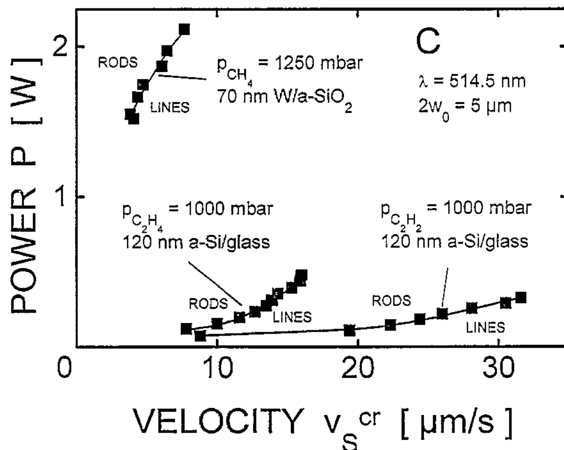

Fig. 6. Critical curves for the deposition of C from C_2H_2, C_2H_4, and CH_4.

4. Conclusions

The transition from uniform (continuous) lines to equidistant fibers originally observed during pyrolytic direct writing of Si lines deposited from SiH_4 seems to be a quite general phenomenon. A similar behavior is found for the deposition of Si from Si_2H_6 and of C from CH_4, C_2H_2, and C_2H_4. Apart from C_2H_2, the transition is discontinuous and shows a hysteresis with respect to laser power and scanning velocity. The boundary between the two regimes in the diagram laser power versus scanning velocity agrees qualitatively with the predictions of a one-dimensional model for laser direct writing. The apparent activation energy for the deposition of Si was determined to be 44.3 and 40.4 kcal/mol for SiH_4 and Si_2H_6, respectively.

Acknowledgements

We wish to thank the "Fonds zur Förderung der Wissenschaftlichen Forschung in Österreich" for financial support.

References

[1] D. Bäuerle, Laser Processing and Chemistry (Springer, Berlin, 1996).
[2] R.B. Jackman, J.S. Foord, A.E. Adams and M.L. Lloyd, J. Appl. Phys. 59 (1986) 2031.
[3] Y.C. Du, U. Kempfer, K. Piglmayer, D. Bäuerle and U.M. Titulaer, Appl. Phys. A 39 (1986) 167.
[4] T. Szörényi, G.Q. Zhang, Y.C. Du, R. Kullmer and D. Bäuerle, in: Laser Processing and Diagnostics (II), Eds. D. Bäuerle, K.L. Kompa and L.D. Laude (Les Editions de Physique, Les Ulis, 1986) p. 91.

[5] D. Braichotte and H. Van den Bergh, Appl. Phys. A 44 (1987) 353.
[6] B. Markwalder, M. Widmer, D. Braichotte and H. Van den Bergh, J. Appl. Phys. 65 (1989) 2470.
[7] S. Preuß and H. Stafast, Appl. Phys. A 54 (1992) 152.
[8] J. Messelhäuser, E.B. Flint and H. Suhr, Appl. Phys. A 55 (1992) 196.
[9] F. Foulon and M. Stuke, Appl. Phys. A 56 (1993) 283.
[10] G. Reisse, F. Gänsicke and A. Fischer, Appl. Surf. Sci. 69 (1993) 412.
[11] C. Garrido and H. Van den Bergh, Jpn. J. Appl. Phys. 32 (1993) 1312.
[12] P.B. Kargl, R. Kullmer and D. Bäuerle, Appl. Phys. A 57 (1993) 175.
[13] J. Han and K.F. Jensen, J. Appl. Phys. 75 (1994) 2240.
[14] P.B. Kargl, R. Kullmer and D. Bäuerle, Appl. Phys. A 57 (1993) 577.
[15] N. Arnold, R. Kullmer and D. Bäuerle, Microelectron. Eng. 20 (1993) 31.
[16] N. Arnold, P.B. Kargl, R. Kullmer and D. Bäuerle, Appl. Surf. Sci. 86 (1995) 457.
[17] R. Kullmer, P. Kargl and D. Bäuerle, Thin Solid Films 218 (1992) 122.
[18] American Institute of Physics Handbook (McGraw-Hill, New York, 1973); Kohlrausch, Praktische Physik 3 (Teubner, Stuttgart, 1968); Landolt–Börnstein, New Series III, Vol. 16a, Ferroelectrics: Oxides (Springer, Berlin, 1981).
[19] N. Arnold, J. Appl. Phys. (1996), to be published.
[20] T. Iwanaga and M. Hanabusa, Jpn. J. Appl. Phys. 23 (1984) L473.
[21] H. Stafast, Appl. Phys. A 45 (1988) 93.
[22] B.A. Scott, in: Semiconductors and Semimetals, Ed. J.I. Pankove, Vol. 21 (Academic Press, New York, 1984) pp. 2, 123.
[23] Landold–Börnstein, New Series III, Vol. 17, Semiconductors (Springer, Berlin, 1991).
[24] J. Doppelbauer and D. Bäuerle, in: Interfaces Under Laser Irradiation, Eds. L.D. Laude, D. Bäuerle and M. Wautelet, Vol.134, NATO ASI Series E (Nijhoff, Dordrecht, 1987) p. 277.
[25] Landold–Börnstein, New Series III, Vol. 15c, Metals, Transport Phenomena (Springer, Berlin, 1991).